scientific reports

Check for updates

OPEN

Synthesis and characterization of Co-MOF@Ag_2O nanocomposite and its application as a nano-organic catalyst for one-pot synthesis of pyrazolopyranopyrimidines

Ghader Hootifard, Enayatollah Sheikhhosseini✉, Sayed Ali Ahmadi & Mahdieh Yahyazadehfar

In this study, a Co-MOF was synthesized via a co-precipitation procedure and then used as support for stabilizing Ag ions and producing Co-MOF@Ag_2O nanocomposite by microwave irradiation. The characterization of synthesized Co-MOF@Ag_2O nanocomposite was performed by using different techniques such as field emission scanning electron microscopy (FE-SEM), energy dispersive X-ray (EDX) analyses, X-ray diffraction (XRD), Thermogravimetric analysis (TGA), Brunauer–Emmett–Teller (BET) and Fourier-transform infrared (FT-IR). The prepared Co-MOF@Ag_2O nanocomposite was applied as a heterogeneous nano-catalyst in the synthesis of pyrazolopyranopyrimidines in water at 50 °C via the one-pot multicomponent reaction of ethyl acetoacetate, hydrazine hydrate, aromatic aldehydes and barbituric acid derivatives. Through this straightforward and effective protocol, different tricyclic fused pyrazolopyranopyrimidines were synthesized at high yields, and short reaction times, through an uncomplicated work-up process with no by-product. The Co-MOF@Ag_2O nanocomposite has been effectively recycled for four consecutive cycles without appreciable loss in its activity. Cost-effectiveness, no need for column chromatography, mild conditions, catalyst recyclability, and eco-friendly nature make it a promising candidate compared to other methods.

The unique characteristics of MOFs such as high surface area, considerable and tunable porosity, tunable pore size and shape, high physical and chemical stability, the presence of active binding sites within the framework, amphiphilic microenvironment, diverse structures, large pore size, nanometer-scale size, and biodegradability[1–3] have caused their importance and application in various industrial and biomedical fields, in which the following can be mentioned: generation of MOF-based metal and metal oxide nanocomposites as heterogeneous catalysts or as catalyst supports/precursors in organic reactions, catalyze a vast range of transformations from organic reaction to photocatalysis[4], as stationary phases for liquid and gas chromatographies and as the efficient adsorption materials in sample pretreatment[5], application as agents' gas and energy storage, heat transformation, imaging, molecular separation, sensing, biosensors, contrast agents for magnetic resonance imaging and etc[6,7].

Among various metal oxides, silver oxide (Ag_2O) is the best candidate for the synthesis of heterogeneous catalysts due to its proper band gap energy (1.2 eV). Silver oxide nanoparticles are p-type semiconductors with vast applications in the field of catalysis, sensors, fuel cells, and photovoltaic cells[8–11]. Many physical and chemical properties such as luminescence, conductivity, and catalytic activity depend on the size of nanoscale materials. Numerous methods have been developed for the preparation of Ag_2O among which, photosensitized reduction, simple chemical method, and electrochemical synthesis can be mentioned[12–14].

Multi-component reactions (MCR) are convergent one-pot processes that enable three or more components to connecting a series of chemical reactions that can lead to enable easy, efficient, automated, and high-throughput synthesis of a wide range of complex natural, heterocyclic, and pharmaceutical structures by combining three or

Department of Chemistry, Kerman Branch, Islamic Azad University, Kerman, Iran. ✉email: sheikhhosseiny@gmail.com; sheikhhosseini@iauk.ac.ir

more substrates[15,16]. Solvent, inter-coordination between the reactants, and catalyst are crucial for the success of MCRs in the sequence of the reaction[17]. The most remarkable attribute of MCRs is that almost all the parts and features of the reactants can be found in the newly formed product indicative of low by-product formation making them wonders of reaction design and efficiency[15]. The development of new MCRs, and improvement of known multi-component reactions are due to their outstanding advantages such as simple operation, high selectivity, high efficiency, high atom economy, reducing the generate of by-products and waste, cost-effectiveness, Saving the chemical materials, time, energy and solvent, eco-friendly nature[18–24].

Fused heterocyclic rings can be abundantly found in nature. One of the most noticeable effects is related to the presence of two or more different moieties in one molecule due to the possibility of possessing the features of all moieties and enhancing pharmacological functions. Recently, considerable developments have been made in the design of new polycyclic heterocycles and fused heterocyclic through combining different motifs of diverse structures. Biological science essentially needs to develop new techniques to synthesize fused heterocyclic compounds[25]. The extensive applications of fused heterocycles comprising pyrimidine, pyran, and pyrazole fragments in pharmaceutics, medicine, and material sciences, along with their biodegradability have raised their popularity[26]. The pyrimidine nucleus significantly contributes to several pharmacological agents with extensive biological functions[27]. Similarly, the pyran nucleus is an important scaffold in different natural production[28]. Moreover, Pyrazole is a necessary heterocycle analog with a critical role in different pharmaceutical and agrochemical processes[29]. Pyrazolopyranopyrimidine and its derivatives are widely used in biological applications. For instance, pyranopyrazole **A** serves as a molluscicidal agent[30]. Pyranopyrazole B is considered a Chk1 inhibitor[31] while pyranopyrazole **C** is an antimicrobial agent[32]. Another instance is the pyrazolopyrimidine core in the popular medicine called sildenafil. Figure 1 shows that the Pyranopyrimidine unit in **D** performs the role of an anti-diabetic agent[33], while pyrazolopyranopyrimidine **E** can provide anti-inflammation effects[34].

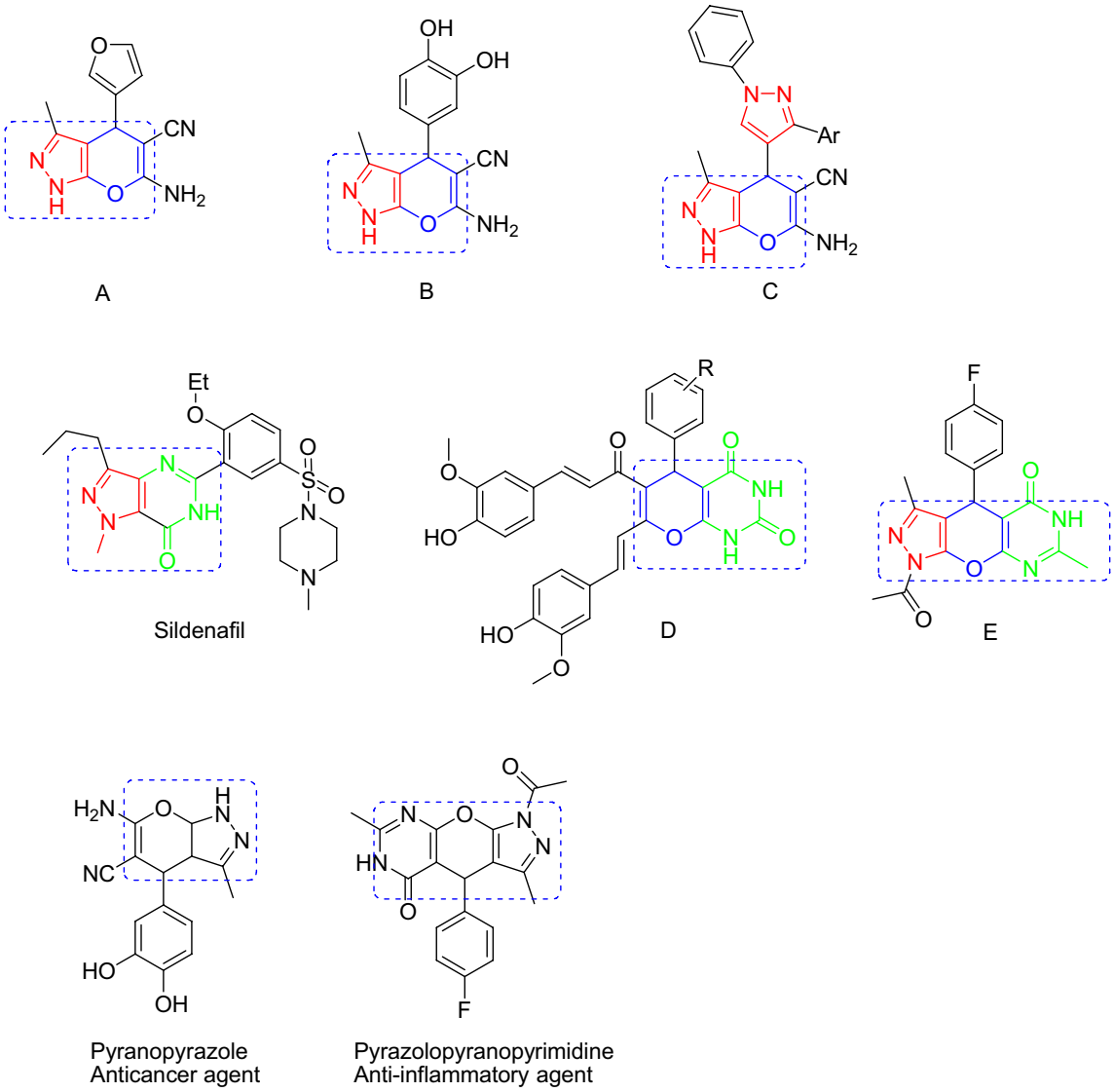

Figure 1. Structure of bio-active pyranopyrazole, pyranopyrimidine, and pyrazolopyranopyrimidine.

As polycyclic heterocycles, pyrazolopyranopyrimidines comprise pyrimidine, pyran, and pyrazole moieties. The pyranopyrimidine fragment has several nature-abundant biological functions such as tyrosine kinase inhibition[35], anticancer features[36], antiallergy[37], antitubercular, antimicrobial, antihypertension[38], antifolates[39], antileishmanial[40], anti-inflammation[41], antibronchitis[42], hypoglycaemic[35], anticonvulsants[43], antidepressants[37], analgesics[41], diuretics[44], hepatoprotection[45], and calcium channel antagonists[46]. Studies have also shown the critical role of the pyranopyrazole fragment in pharmaceutical and agrochemical industries[30] while representing interesting patterns in pharmaceutics and valuable contributions to various biological functions of molecules.

The synthesis of pyrazolopyranopyrimidines mainly involves the four-component condensation of aryl aldehydes, barbituric acid derivatives, ethyl acetoacetate, and hydrazine hydrate. As shown by previous studies, pyrazolopyranopyrimidines can be prepared through the application of different catalytic agents, including SDS[47], DABCO[48], ChCl:Urea[49], Halloysite clay nanotubes[50], Magnetized Water[51], Nano-ZnO[52], TiO_2 nanowire[53], Meglumine[54], cellulose-based nanocomposite[55], silica-bonded (SB DBU^+Cl^-), (SB-$DABCO^+Cl^-$), (NSB-DBU^+Cl^-)[56], MNS-ionic liquid[57], OMWC nanotubes[58], SBA-PR-SO_3H[59], oleic acid[60], and Cu-IMS nanoparticles[61].

Each of these catalytic systems has simultaneously their own advantages and disadvantages for catalyzing this reaction. Some of them suffer from disadvantages such as long reaction time[58,61] and hard preparation process to prepare the catalyst[50]. Hence, there is still a need for more attempts to design and explore new and more efficient catalytic systems with tailored functional groups, that address green and sustainable chemistry principles. In this regard, the current study applied Co-MOF@Ag_2O in a green medium to develop a safe protocol for the synthesis of pyrazolopyranopyrimidine derivatives. The novelty of this precedure is the synthesis of a new and recyclable Co-MOF@Ag_2O nano-catalyst and using it in preparation of the heterocyclic synthesis in organic reaction efficiently.

Experimental section

Chemicals and reagents

Silver nitrate, cobalt(II) nitrate, dimethylformamide, 2,6-pyridinedicarboxylic acid, ethanol, sodium hydroxide, Hydrazine hydrate, ethyl acetoacetate, aryl aldehydes, and barbituric acid derivatives were purchased from Sigma-Aldrich. The chemicals were used without further purification.

Material characterization

Melting point (m.p.) measurement was performed by an open capillary tube method using an electrothermal 9200 apparatus. Reactions were monitored by TLC. FT-IR spectra were obtained as potassium bromide pellets in the range of 400–4000 cm^{-1} on a Bruker FT-IR Tensor 27 spectrophotometer. Nuclear magnetic resonance (NMR) spectra were obtained on a Bruker DRX-400 Avance instrument (400 MHz for ^1H) with DMSO-d_6 as solvent. Chemical shifts were expressed in parts per million (ppm), and coupling constant (J) was reported in hertz (Hz). All the known compounds were identified by comparison of their melting points with the corresponding values in the literature. A Philips analytical PC-APD X-ray diffractometer operating with Kα radiation (α_2, $\lambda_2 = 1.54439$ Å) and graphite mono-chromatic Cu radiation (α_1, $\lambda_1 = 1.54056$ Å) was employed for the X-ray powder diffraction (XRD) analysis to assess the crystalline condition of the product. Then, scanning electron microscopy equipped with an energy-dispersive X-ray spectroscope (KYKY & EM 3200) was utilized for morphological investigation of the Co-MOF@Ag_2O nanocomposite. Thermal behavior was analyzed in N_2 from room temperature to 350 °C using a STA-1500 thermoanalyzer. N_2 adsorption–desorption isotherms (BET) were measured on a TriStar II Plus surface area and porosity analyzer at 77 K.

Synthesis of Co-MOF@Ag_2O nanocomposite

Synthesis of Ag_2O nanoparticles

Synthesis of Ag_2O nanoparticles involved the dissolution of 0.005 mmol of silver nitrate in 80 mL deionized water, followed by the dropwise addition of 20 mL of 0.025 NaOH which immediately led to precipitation. Finally, the products were separated and rinsed with distilled water for 30 min, and dried in an oven at 130 °C[62].

Synthesis of Co-MOF

8.186 mmol cobalt(II) nitrate was added to the solution of 2,6-pyridinedicarboxylic acid-linker (3.101 g) in the least volume of dimethylformamide, followed by 8 h of stirring at 100 °C. The resulting Co-MOF precipitates were finally collected and the residual raw materials were eliminated by washing with dimethylformamide and ethanol three times followed by 12 h of drying at 100 °C[63,64].

Synthesis of Co-MOF@Ag_2O nanocomposite

Synthesis of Co-MOF@Ag_2O nanocomposite involved dispersion of a 0.6 g powder of the dried Co-MOF in deionized water followed by adding 0.179 g (1 mmol) of Ag_2O under stirring at 80 °C for 10 min to reach a homogeneous solution. The final powder mixture was transferred to a glassy vial for microwave irradiation. (300 W) for 70 min. The raw materials were eliminated by washing with acetic acid. The dried powder was calcined in a furnace at 170 °C.

General procedure for the synthesis of pyrazolopyranopyrimidines

Hydrazine hydrate (1.0 mmol), ethyl acetoacetate (1.0 mmol), aldehyde (1.0 mmol), and barbituric acid (1.0 mmol) were added to a 50 mL round-bottom flask containing Co-MOF@Ag_2O (20 wt%, 0.030 g) and water (5.0 mL) and stirred at 50 °C. The progress of the reaction was monitored by thin- layer chromatography. After completion of the reaction, the mixture was filtered, then the resulting precipitate was dissolved in hot ethanol

and the Co-MOF@Ag_2O nano-catalyst was separated by filtration. The solution was concentrated by solvent evaporation and the resulting precipitate was washed with water to achieve pure products. The catalyst was recovered by separation followed by washing with water and acetone (5 mL) twice to be reused after drying in an oven at 65 °C.

Selected spectral data

4-(2-hydroxynaphthalen-1-yl)-3-methyl-4,8-dihydropyrazolo[4',3':5,6]pyrano[2,3-d]pyrimidine-5,7(1H,6H)-dione (5r): Yield 90%, m.p: 220–221 °C; ^{1}H NMR (400 MHz, DMSO-d_6, ppm): δ 2.62 (s, 3H, CH_3), 5.35 (s, 1H, CH), 7.38 (d, 1H, J_1 = 9.2 Hz), 7.51–7.55 (m, 2H, 1H-Ar, 1H-NH), 7.62 (td, 1H, J_1 = 15.6 Hz, J_2 = 1.2 Hz, H-Ar), 7.70 (td, 1H, J_1 = 15.6 Hz, J_2 = 1.2 Hz, H-Ar), 7.97 (d, J = 8.8 Hz, 1H, H-Ar), 8.11 (d, J = 9.2 Hz, 1H, H-Ar), 8.74 (s, 1H, OH), 10.09 (s, 1H, NH), 12.98 (s, 1H, NH) ppm; ^{13}C NMR (100 Hz, DMSO-d_6): δ 10.0, 23.3, 87.9, 108.4, 116.4, 118.9, 121.8, 123.8, 124.9, 127.0, 128.0, 129.0, 130.7, 131.0, 132.3, 134.7, 160.0, 161.3 ppm.

Results and discussion

Characterization of Co-MOF@Ag_2O nanocomposite

Scanning electron microscopy (SEM) image shows (Fig. 2) the morphological features of Co-MOF@Ag_2O nanocomposite. This image shows the formation of aggregated spherical Co-MOF@Ag_2O nanocomposite particles with a size range of 11 to 30 nm.

Energy-dispersive X-ray spectroscopy (EDX) results show the elemental analysis of Co-MOF@Ag_2O nanocomposite (Fig. 3). The strong signal at 3 keV can be assigned to silver while some weak signals can be seen related to Co, N, O, and C. The major emission energy at 3 keV indicates the presence of silver.

X-ray diffraction patterns of annealed samples are depicted in Fig. 4. The XRD patterns reveal the polycrystalline nature of the synthesized Ag_2O nanoparticles with cubic phase. The observed diffraction peaks correspond to (111), (200), (220), and (311) planes and well match with standard data of face-centered cubic silver (JCPDS Card No. 04-0783)[51]. Figure 3 also shows the XRD pattern of Co-MOF which indicates multiple diffraction peaks, suggesting the poly-crystalline structure of Co-MOF. The crystallite size was estimated by Scherrer's formula $D = K\lambda/\beta\cos\theta$.

Where K = 0.9 (constant), λ = 1.54 Å, β is the Full Width at Half Maximum (FWHM) calculated in radians and θ denotes the Bragg's diffraction angle. The average crystallite size of the Co-MOF@Ag_2O nanocomposite was 28.2 nm with excellent dispersity.

The thermogravimetric analysis (TGA) indicates a continuous mass loss of Co-MOF@Ag_2O nanocomposite before ca. 420 °C (Fig. 5). The weight loss around 100 °C (weight loss: 6.51%) can be related to the evaporation of solvent, while the weight loss between 241 and 373 °C (weight loss: 26.43%) is due to the decomposition of the ligand. The weight loss in the range of 375–478 °C (weight loss: 7.23%), may be attributed to the decomposition of coordinated water. The relatively high thermal decomposition temperature shows that Co-MOF@Ag_2O nanocomposite has good thermal stability properties.

The porous characteristics of the Co-MOF@Ag_2O nanocomposite were investigated by isothermal nitrogen adsorption–desorption measurements. Figure 6A depicts a typical IV isotherm with a distinct hysteresis loop in the range of 0.39–1.0 pp_0^{-1}, suggesting the mesoporous structure of the nanocomposite. The pore size distribution was calculated by desorption isotherm via the Barret–Joyner–Halenda (BJH) method as shown in Fig. 6B. The as-synthesized Co-MOF@Ag_2O nanocomposite exhibited narrow pore-size distribution centered at ~ 5.38 nm,

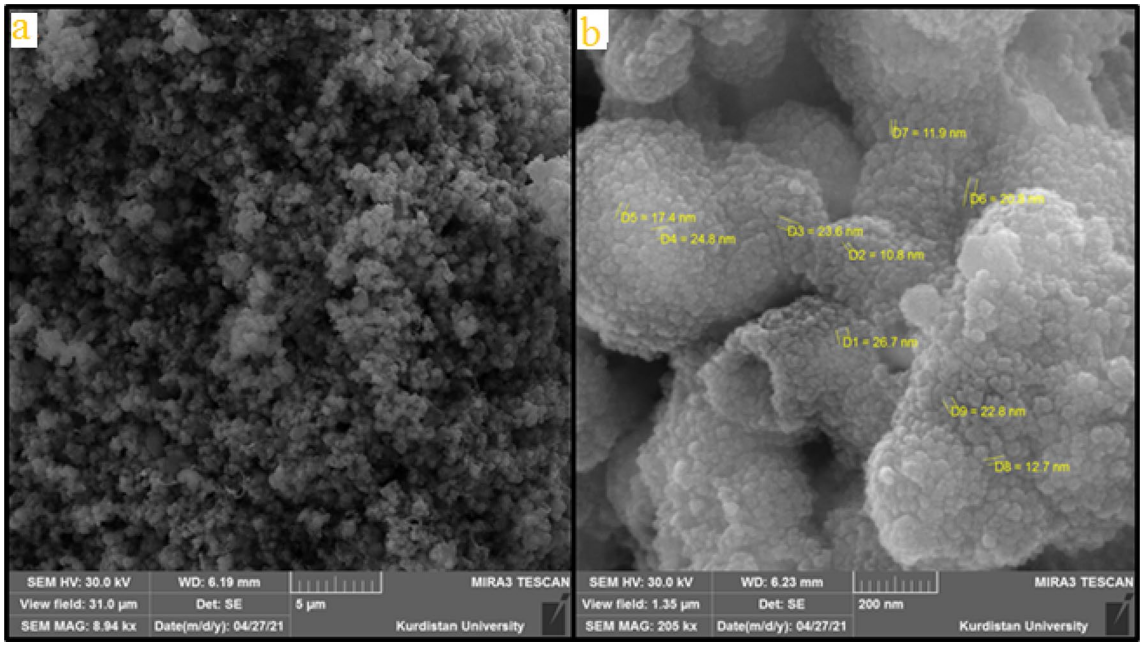

Figure 2. (**a**) FE-SEM image and (**b**) high-resolution FE-SEM image of the Co-MOF@Ag_2O nanocomposite.

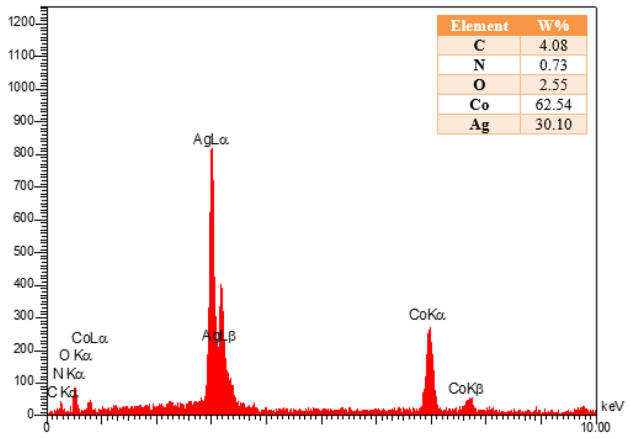

Figure 3. EDX spectra of Co-MOF@Ag_2O nanocomposite.

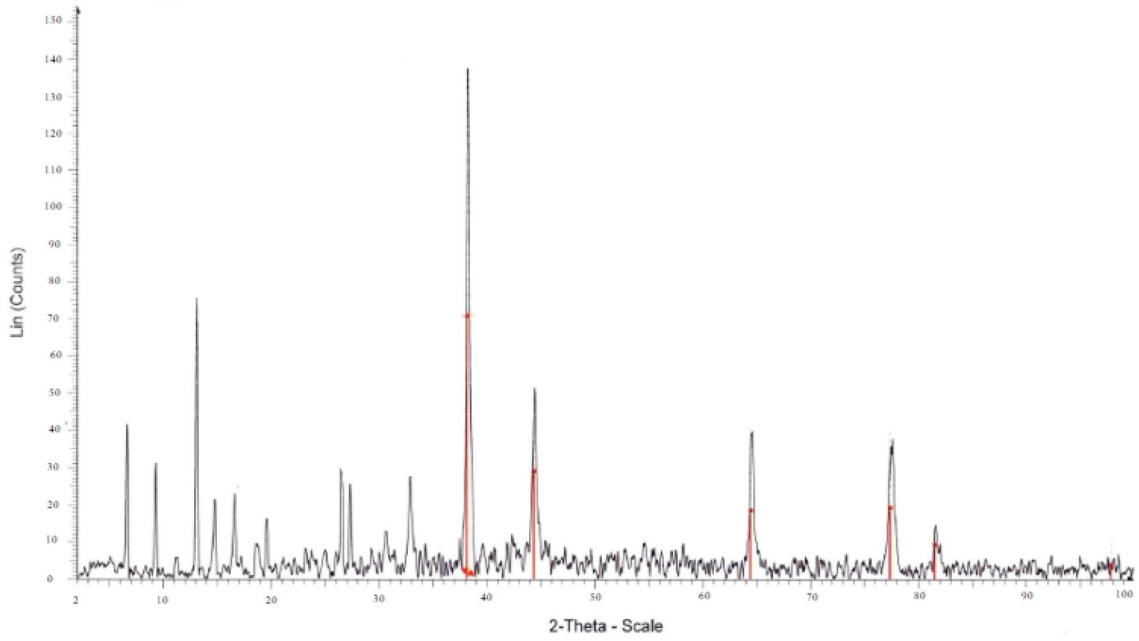

Figure 4. XRD pattern of Co-MOF@Ag_2O nanocomposite.

which further confirm the mesoporous structure of the nanocomposite. The Brunauer–Emmett–Teller (BET) specific surface area and pore volume of the nanocomposite were 81.613 $m^2\ g^{-1}$ and 0.12 $cm^3\ g^{-1}$, respectively. The formation of the mesopores was confirmed by the gas release during the decomposition of the precursor.

The FT-IR spectra of Ag_2O, 2,6-pyridinedicarboxylic acid linker, Co-MOF, and Co-MOF@Ag_2O are shown in Fig. 7. In the IR spectrum of Ag_2O NPs (7a), the peaks at 703 and 882 cm^{-1} can be attributed to the vibrations of Ag–O whereas the wide band at 431 cm^{-1} can be ascribed to Ag metal.

The FTIR spectrum of 2,6-pyridinedicarboxylic acid linker (7b) shows peaks at 3451, 1413, and 1460 cm^{-1} are related to the stretching vibrations of ∂(OH), C-O, and C-N groups, respectively. The symmetric and asymmetric stretching vibrations of aromatic carboxylates also appeared at 1413–1695 cm^{-1}. The peak at 3067 cm^{-1} suggests the presence of free ligand resulting from protonation of the uncoordinated pyridinium ion in the former, and strong hydrogen bonding in the latter[65].

According to the spectrum of (7c), the peaks emerging at 3483, 3421, 3242, 1573, and 1429 cm^{-1} and those at 1076 cm^{-1} confirmed the presence of the coordinated water, carboxyl group, stretching vibration of C–H, COO group, stretching vibration of C–O bonds, and stretching vibration of (C–C) in the Co–MOF structure, respectively. The peaks at 1008 cm^{-1} can be also assigned to Co–CH and Co in the final Co–MOF nanostructures. The band at ~ 729–943 cm^{-1} can be attributed to the Co–O in the final MOF nanostructures[66].

One of the signs of the formation of the Co–MOF with the addition of cobalt nitrate to the linker is the reduction of carbonyl absorption due to the coordination of the cobalt metal with the oxygen of the carbonyl groups of the linker.

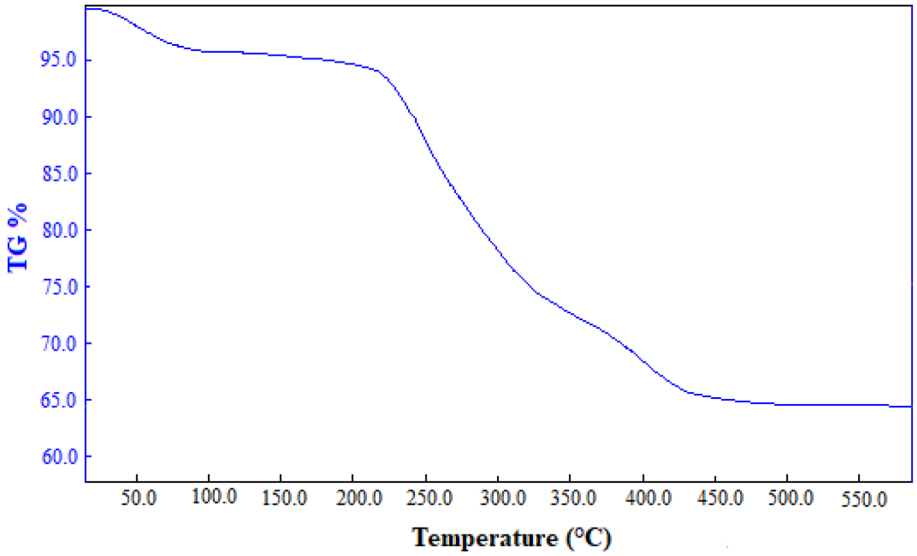

Figure 5. TGA analysis of Co-MOF@Ag_2O nanocomposite.

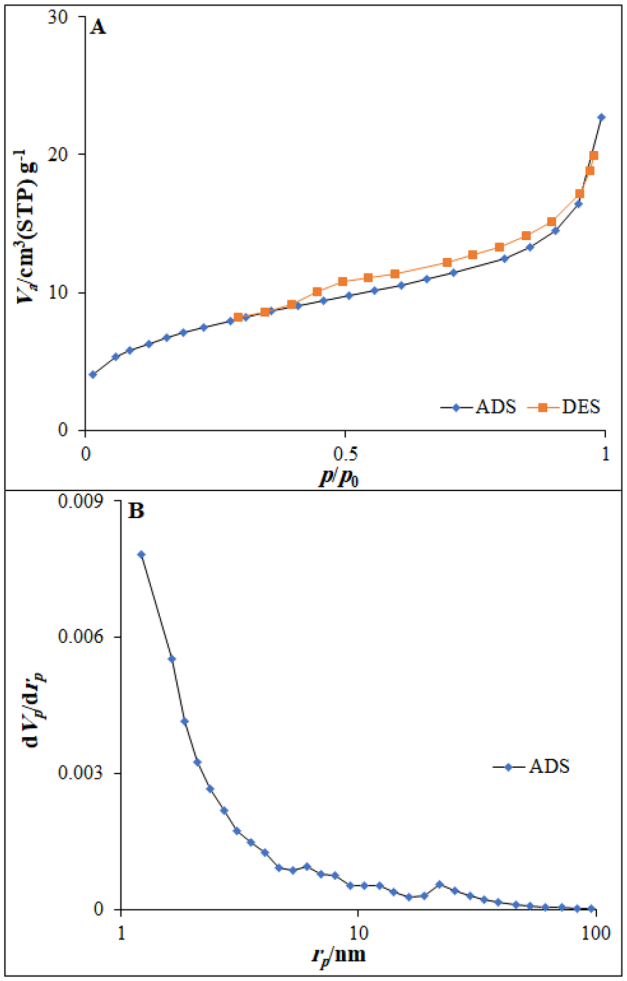

Figure 6. (**A**) N_2 adsorption–desorption isotherms Co-MOF@Ag_2O nanocomposite and (**B**) BJH results obtained for Co-MOF@Ag_2O nanocomposite.

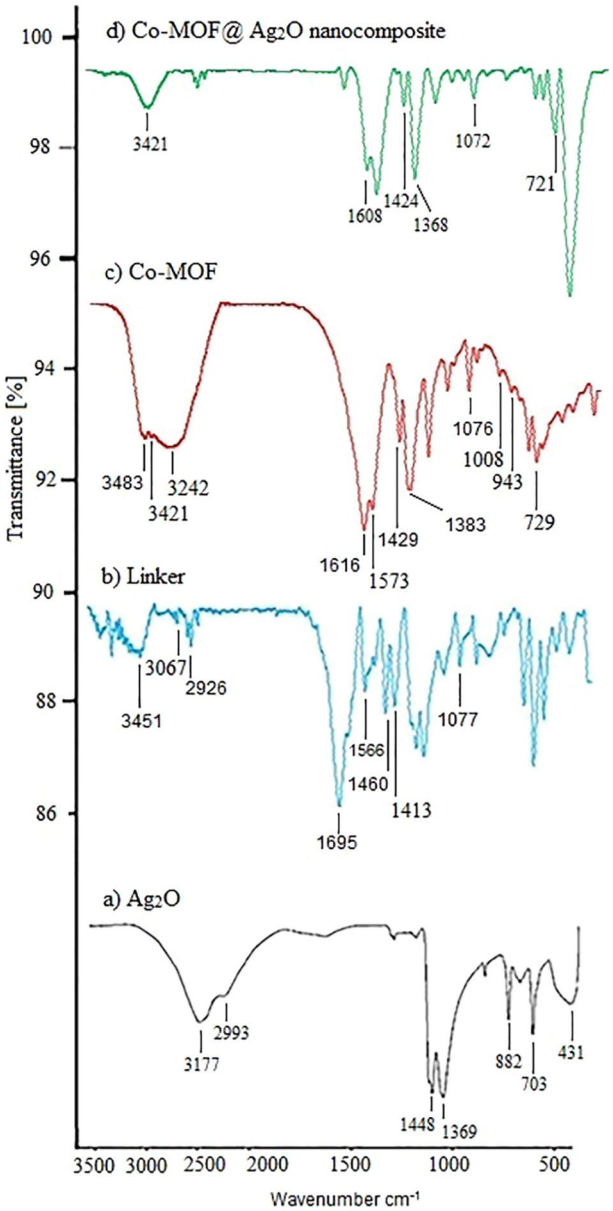

Figure 7. IR (KBr, υ/cm^{-1}) curve of (**a**) Ag_2O, (**b**) 2,6-pyridinedicarboxylic acid linker, (**c**) synthesized Co-MOF and (**d**) Co-MOF@Ag_2O nanocomposite.

In the IR spectrum of (7d), a peak at 721 cm^{-1} indicates the presence of Ag_2O NPs in the final composite. Moreover, the absorption of carbonyl showed a decrease due to the coordination of the Ag_2O nanoparticle with the oxygen of the carbonyl group. These two signs confirm the presence of silver nanoparticles in the Co-MOF structure and its contribution to the formation of the Co-MOF@Ag_2O complex.

Synthesis of dihydropyrazolopyranopyrimidine diones in the presence of Co-MOF@Ag_2O as nano-organocatalyst

As shown in Fig. 8, the optimum reaction conditions for the synthesis of pyrazolopyranopyrimidine in the presence of Co-MOF@$A_{g2}O$ catalyst involves the one-pot four-component reaction of ethyl acetoacetate, hydrazine hydrate, 3-nitro benzaldehyde, and barbituric acid.

First, the impacts of the catalyst loading were examined within the model reaction at 50 °C and water as the medium. In such conditions, 20 wt% of the catalyst was the optimal content to complete the reaction with higher efficiency and shorter reaction time (Table 1, entry 5). No effects were reported on the product efficiency when the catalyst amount was increased (Table 1, entries 6, 7), while the desired product showed a lower yield when lower percentages of Co-MOF@Ag_2O were employed (Table 1, entries 2, 3, and 4). The four-component reaction was conducted in water at 50 °C with no catalytic agent to find the actual effectiveness of the catalyst. The results of Table 1 (entry 1) indicated the achievement of the trace product even after 2 h of reaction.

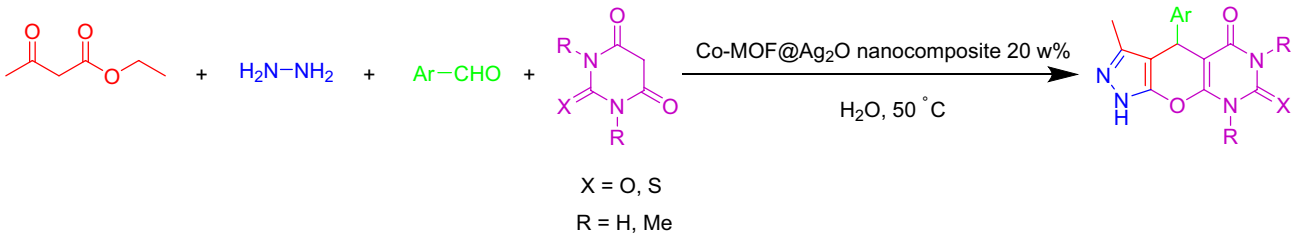

Figure 8. Four-component synthesis of pyrazolopyranopyrimidines catalyzed by Co-MOF@Ag_2O in water at 50 °C.

Entry[a]	Catalyst	Solvent	Tem (°C)	Time (min)	Yield[b] (%)
1	–	H_2O	50 °C	120	Trace
2	Co-MOF@Ag_2O 5%	H_2O	50 °C	10	75
3	Co-MOF@Ag_2O 10%	H_2O	50 °C	10	80
4	Co-MOF@Ag_2O 15%	H_2O	50 °C	4	83
5	Co-MOF@Ag_2O 20%	H_2O	50 °C	3	96
6	Co-MOF@Ag_2O 25%	H_2O	50 °C	3	96
7	Co-MOF@Ag_2O 30%	H_2O	50 °C	3	97
8	Co-MOF@Ag_2O 20%	CH_3CN	50 °C	57	67
9	Co-MOF@Ag_2O 20%	DMF	50 °C	45	72
10	Co-MOF@Ag_2O 20%	MeOH: H_2O	50 °C	14	79
11	Co-MOF@Ag_2O 20%	EtOH: H_2O	50 °C	10	88
12	Co-MOF@Ag_2O 20%	EtOH	50 °C	25	79
13	Co-MOF@Ag_2O 20%	MeOH	50 °C	45	71
14	Co-MOF@Ag_2O 20%	Solvent free	50 °C	12	63
15	Co-MOF@Ag_2O 20%	H_2O	r.t.	145	Trace
16	Co-MOF@Ag_2O 20%	H_2O	70 °C	2	98

Table 1. Optimization of the reaction conditions for the synthesis of pyrazolopyranopyrimidines using Co-MOF@Ag_2O nanocomposite. [a]Reaction conditions: 3-nitrobenzaldehyde (1 mmol), barbituric acid (1 mmol), ethyl acetoacetate (1 mmol), hydrazine hydrate (1 mmol) in presence of Co-MOF@Ag_2O nanocomposite and solvent (10 mL). [b]Yield refers to isolated products.

Table 1 also indicates temperature effects on the conversion, revealing a low product yield at room temperature (Table 1, entry 15). The product yield improved significantly by raising the temperature from room temperature to 50 °C. However, as shown in Table 1 (entry 16), further temperature elevation from 50 to 70 °C caused no changes in the product yield and reaction time.

Different solvents, including polar aprotic (DMF, CH_3CN) and polar protic (H_2O, MeOH, EtOH, EtOH–water, and MeOH–water mixture) were used to conduct the model reaction and examine the effects of the solvent. Water showed the highest effectiveness as the solvent, leading to the smooth proceeding of the four-component reaction at the greatest yield. Significant changes were observed in the reaction profile by changing to the aprotic polar solvent acetonitrile, prolonging the reaction. The use of protic solvents affected the reaction positively through hydrogen bonding with the substrates. Besides, the hydrophobic effects of water may justify the superiority of water compared to ethanol. Another point is the low yield of the target product when performing the reaction in solvent-free conditions (Table 1, entry 14), confirming the high reliance of the reaction on the solvent.

According to Table 2, different barbituric acids and aldehydes with electron-donating and withdrawing groups were used to examine the scope and generality of the proposed technique by performing the reaction at optimum conditions. As shown, excellent yields were obtained by all benzaldehyde derivatives. Yet, slightly greater yields were achieved in the case of the electron-withdrawing group. Moreover, an 84% product yield was reported when three electron-donating methoxy groups were present on the aromatic ring of the aldehyde (Table 2, entry 18). On the other hand, the yield of the reaction with barbituric acid was slightly higher than thiobarbituric acid and N, N-dimethyl barbituric acid because of less sterically challenging barbituric acid. The product 5r was characterized in terms of melting point and spectral data, such as FT-IR and NMR spectra.

Figure 9 shows the proposed Co-MOF@Ag_2O-catalyzed mechanisms to synthesize pyrazolopyranopyrimidine derivatives from ethyl acetoacetate, hydrazine hydrate, benzaldehyde, and barbituric acid. The process represented a typical Knoevenagel condensation cascade followed by Michael addition and cyclization Co-MOF@Ag_2O. Initially, the carbonyl group in ethyl acetoacetate (2) that activated by catalyst was attacked by hydrazine hydrate (1).

Entry[a]	Aldehyde	R	X	Product	Time (min)	Yield (%)[b]	m.p. (°C)	
							Found	Reported [ref.]
1	3-$NO_2C_6H_4^-$	H	O	5a	10	92	268–270	266–267[54]
2	2-$NO_2C_6H_4^-$	H	O	5b	6	90	208–210	208–209[54]
3	4-$NO_2C_6H_4^-$	H	O	5c	4	92	231–233	233–234[54]
4	$C_6H_5^-$	H	O	5d	6	96	219–220	218–219[54]
5	$C_6H_5^-$	H	S	5e	5	94	222–223	220–221[54]
6	$C_6H_5^-$	Me	O	5f.	5	93	194–195	192–193[54]
7	4-$ClC_6H_4^-$	H	O	5 g	11	98	222–223	222–223[54]
8	4-$ClC_6H_4^-$	Me	O	5 h	13	94	199–201	199–200[54]
9	4-$ClC_6H_4^-$	H	S	5i	9	95	231–233	232–239[67]
10	4-$BrC_6H_4^-$	H	O	5j	5	96	210–211	211–212[67]
11	2-$CH_3C_6H_4^-$	H	O	5 k	8	92	261–264	260–262[68]
12	4-$CH_3C_6H_4^-$	H	O	5 l	7	94	198–201	200–201[54]
13	4-$CH_3C_6H_4^-$	Me	O	5 m	10	89	172–174	172–173[54]
14	4-$CH_3C_6H_4^-$	H	S	5n	9	89	219–221	219[59]
15	4-$OCH_3C_6H_4^-$	H	O	5o	6	91	227–229	225–227[69]
16	4-$OCH_3C_6H_4^-$	H	S	5p	8	88	222–223	224–226[70]
17	4-$OCH_3C_6H_4^-$	Me	O	5q	10	86	175–177	175–177[70]
18	3,4,5-$(OCH_3)_3C_6H_2^-$	H	O	5r	12	84	248–249	248–250[68]
19	2-$OHC_6H_4^-$	H	O	5 s	5	94	263–265	264–266[68]
20	4-$OHC_6H_4^-$	H	O	5q	5	95	263–267	262–264[68]
21	2-OH-1-naphthaldehyde	H	O	5r	14	90	220–221	–

Table 2. Preparation of pyrazolopyranopyrimidines in the presence of Co-MOF@Ag_2O (20 w%) under optimized reaction conditions. [a]Reaction conditions: Aryl aldehydes (1 mmol), barbituric acid derivatives (1 mmol), ethyl acetoacetate (1 mmol) hydrazine hydrate (1 mmol) in the presence of Co-MOF@Ag_2O were heated in H_2O at 50 °C for appropriate times. [b]Yield refers to isolated products.

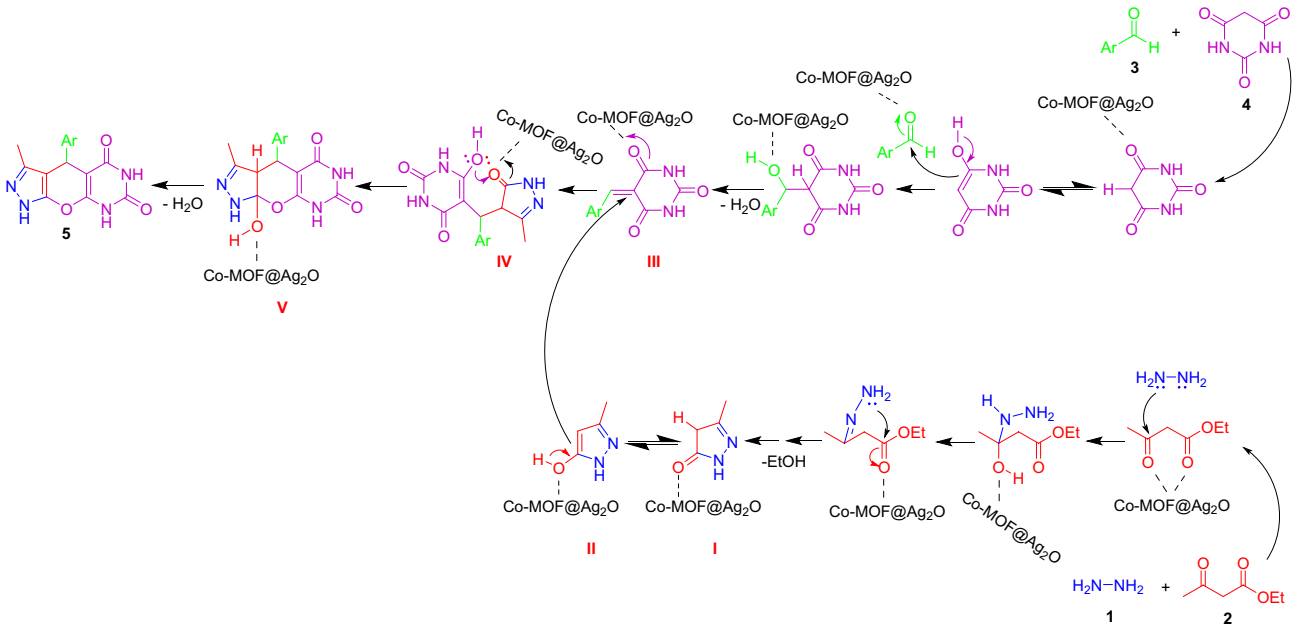

Figure 9. The proposed mechanism for synthesis of pyrazolopyranopyrimidines.

The resulting adduct condensation was converted to intermediate I as it lost a molecule of water; then, EtOH was tautomerized to its relative equilibrium enolate form II in the presence of Co-MOF@Ag_2O. Yet, Knoevenagel condensation of activated aldehyde and barbituric acid in the presence of Co-MOF@Ag_2O led to the formation of intermediate III. Then, the reaction of intermediate (II) occurs with the Knoevenagel condensate (III) product through a Michael addition reaction to produce intermediate (IV). The nucleophilic addition of the enolate oxygen to the activated carbonyl group leads to the intramolecular cyclization of intermediate (IV) and

afforded intermediate (V). In the last step, the Co-MOF@Ag_2O catalyst assists intermediate V to lose a water molecule and form target product 5.

Table 3 summarizes the previous procedures used to synthesize fused tricyclic pyrazolopyranopyrimidine derivatives, highlighting the value of the proposed catalyst compared to others. For this purpose, preparation of 3-methyl-4-phenyl-4,8-dihydropyrazolo[4′,3′:5,6]pyrano[2,3-d]pyrimidine-5,7(1H,6H)-dione (5d) using Co-MOF@Ag_2O was compared with other reported methods. As illustrated, some previously used procedures required higher temperatures, longer reaction times, and challenging processes to prepare the catalyst at proper product yield.

One of the best results was reported for Co-MOF@Ag_2O in water as a catalyst, being operationally simple and recyclable, requiring a shorter reaction time, leading to excellent yields, and a wide substrate range with high functional group tolerance. The two features of cost-effectiveness and the use of water as a green solvent show the superiority of this catalyst over previous catalysts.

The reusability and stability of Co-MOF@Ag_2O nanocatalysts have an important role in determining the economic feasibility of pyrazolopyranopyrimidines production at a large industrial scale. Therefore, the reusability of the Co-MOF@Ag_2O nano-catalyst was investigated for the reaction of 3-nitrobenzaldehyde, barbituric acid, ethyl acetoacetate and hydrazine hydrate as model reaction to produce 5a. After completion of the reaction (monitored by TLC), with separating the obtained precipitates by filtration and dissolving them in ethanol, the Co-MOF@Ag_2O nano-catalyst was separated, washed with water and ethanol (5 mL) and dried in oven at 65 °C for 6 h. It was used in the next reaction. The results depicted that Co-MOF@Ag_2O nano-catalyst can be reused up to 4 times. After being used more than 4 times, Co-MOF@Ag_2O nano-catalyst lost activity gradually (Fig. 10).

The loss of catalytic activity of nano-catalysts may be ascribed to its structural changes. The FE-SEM micrograph of the nano-catalyst (Fig. 11) confirmed the stable surface for the products.

Furthermore, we have characterized the reused nano-catalyst by EDX and FT-IR analyses which EDX analysis showed the presence of carbon, nitrogen, oxygen, cobalt, and silver elements in the reused nano-catalyst. This analysis result is shown in Fig. 12.

In FT-IR spectrum Fig. 13, The existence of a similar pattern including the absorptions of 3421 and 3455 cm^{-1} related to the hydroxyl groups in the Co-MOF@Ag_2O nano-catalyst, the absorptions of 721 and 725 cm^{-1} related to Ag–O vibrations in Ag_2O NPs, the absorptions of the carbonyl groups in linker at 1608 and 1600 cm^{-1} and the absorptions of 1368–1573 cm^{-1} and 1360–1577 cm^{-1} related to the aromatic ring, confirming no change in the structure of the Co-MOF@Ag_2O nano-catalyst.

Entry	Catalyst	Amount of catalyst	Conditions	Time (min)	Yield (%)	Ref.
1	[BNPs-Caff] HSO_4	0.1 g	H_2O, 50 °C	40	95	[71]
2	MNPs@DABCO$^+Cl^-$	0.01 g	Solvent free, 80 °C	5	94	[72]
3	DABCO	20 mol%	H_2O, Reflux	20	99	[48]
4	Meglumine	0.1 mmol	H_2O, r.t	5	97	[54]
5	[MerDABCO-SO_3H] Cl	5 mg	H_2O, 80 °C	5	97	[73]
6	HPA-F-HNTs	0.03 g	H_2O, Reflux	35	96	[50]
7	TEDA/IMIZ-BAIL@UiO-66	0.05 g	EtOH, Reflux	40	93	[74]
8	Cu^{2+}@MSNs-$(CO^{2-})_2$	1.3 mol%	H_2O, r.t.	60	90	[61]
9	Oleic acid	12.5 mol%	EtOH, Reflux	15	78	[60]
10	TiO_2 NWs	10 mol%	EtOH: H_2O, reflux	60	95	[53]
11	SBA-Pr-SO_3H	0.02 g	H_2O, Reflux	10	92	[59]
12	CO-MOF@Ag_2O	20 w%	H_2O, 50 °C	10	92	This work

Table 3. The comparison of the catalytic activity of Co-MOF@Ag_2O with previously reported catalysts.

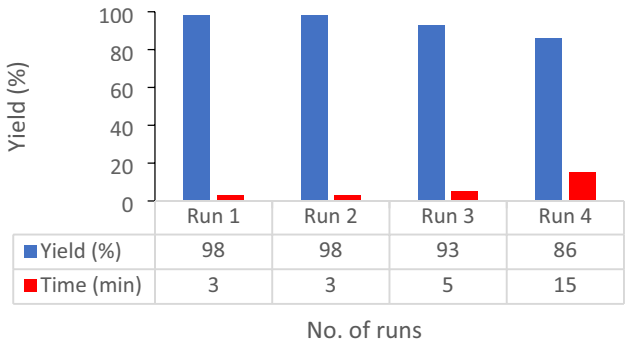

Figure 10. Reusability of catalyst.

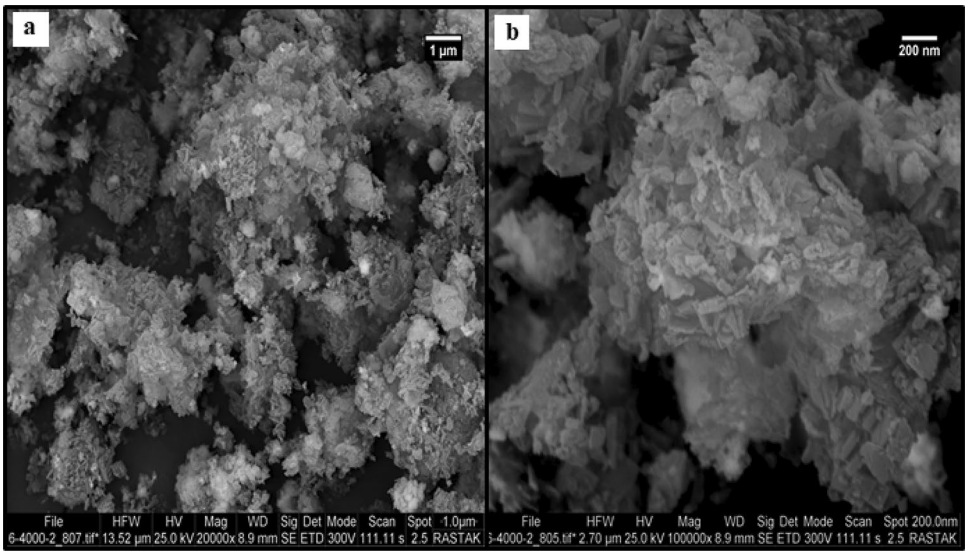

Figure 11. (**a**) FE-SEM image and (**b**) high-resolution FE-SEM image of Co-MOF@Ag_2O nano-catalyst showing change on the catalyst surface structure during the last run (4th) reuse cycle.

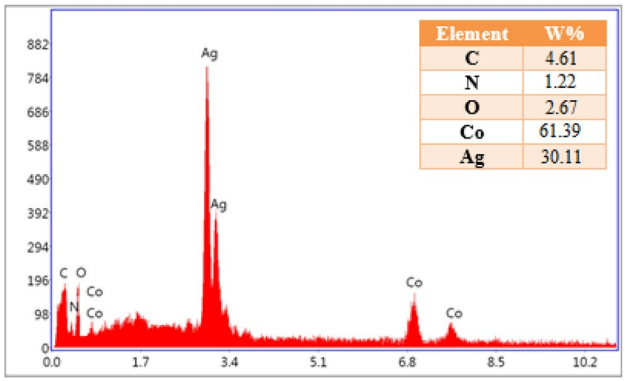

Figure 12. EDX spectra of Co-MOF@Ag_2O nano-catalyst during the last run (4th) reuse cycle.

To approve the heterogeneous nature of the Co-MOF@Ag_2O nanocomposite and the chances of leaching of metal cites of catalyst in the reaction mixture a hot filtration test was performed for the synthesis of pyrazolopyranopyrimidines using 3-nitrobenzaldehyde, barbituric acid, ethyl acetoacetate and hydrazine hydrate as model reaction to produce 5a under the optimized reaction condition. After half time of the reaction (5 min), the reaction was stopped, and the corresponding product was obtained in 71% of yield. The Co-MOF@Ag_2O nanocomposite was separated and removed from the reaction by dissolving precipitates in ethanol and simple filtration. After evaporating the ethanol from the reaction residue, the rest of the reaction was stirred in the catalyst-free conditions for another 5 min. Surprisingly, we observed that low conversion (< 5%) of the product happened through the heating of the catalyst-free mixture for another 5 min which may be a result of the thermal energy applied. It can be concluded that the catalyst has high stability, no active metal centers were leached from the nanocomposite surface.

Conclusion

In conclusion, a nanocatalyst was constructed using Ag_2O nanoparticles which stabilized on the surface of Co-MOF using microwave irradiation and was applied after identification and characterization by SEM, EDX, XRD, TGA, BET, and FT-IR analysis for the preparation of pyrazolopyranopyrimidine heterocycles through a one-pot four-component reaction of ethyl acetoacetate, hydrazine hydrate, aryl aldehydes, and barbituric acid derivatives under solvent-free conditions at 50 °C. The synthesized nano-catalyst in this work indicates more catalytic activity in comparison with the previously proposed procedures. The convenient preparation process, catalyst recyclability, considerable atom economy, and solvent-free and green reaction conditions are among the main strengths of the proposed protocol in this research.

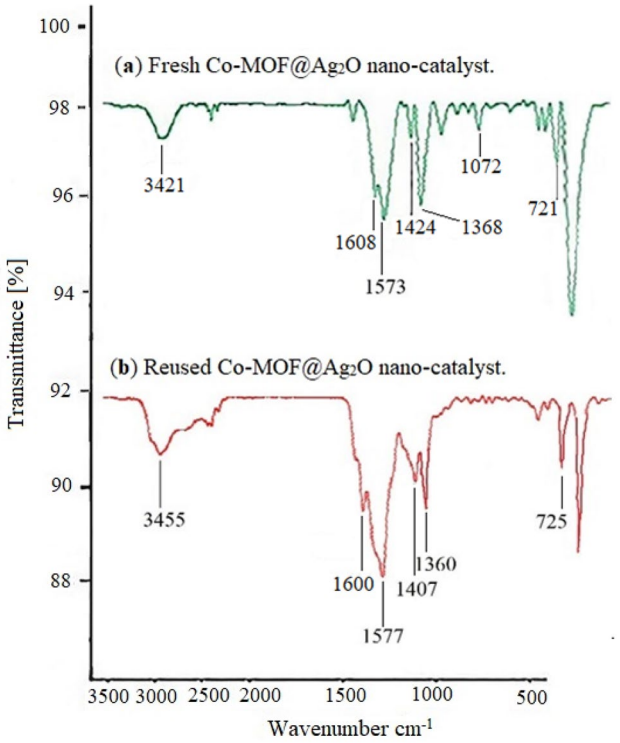

Figure 13. (**a**) FT-IR spectra of fresh Co-MOF@Ag_2O nano-catalyst and (**b**) FT-IR spectra of Co-MOF@Ag_2O nano-catalyst during the last run (4th) reuse cycle.

Data availability

The original contributions presented in the study are included in the article/Supplementary material; further inquiries can be directed to the corresponding author.

Received: 9 May 2023; Accepted: 11 October 2023
Published online: 15 October 2023

References

1. Kumar, S. *et al.* Green synthesis of metal–organic frameworks: A state-of-the-art review of potential environmental and medical applications. *Coord. Chem. Rev.* **420**, 213407. https://doi.org/10.1016/j.ccr.2020.213407 (2020).
2. Li, X., Yang, X., Xue, H., Pang, H. & Xu, Q. Metal–organic frameworks as a platform for clean energy applications. *J. Energy Chem.* **2**, 100027. https://doi.org/10.1016/j.enchem.2020.100027 (2020).
3. Xu, Y., Li, Q., Xue, H. & Pang, H. Metal-organic frameworks for direct electrochemical applications. *Coord. Chem. Rev.* **376**, 292–318. https://doi.org/10.1016/j.ccr.2018.08.010 (2018).
4. Taghavi, R. & Rostamnia, S. Schiff-base post-synthetic modification of IRMOF-3 to encapsulate Pd nanoparticles: It's application in C–C bond formation cross coupling Suzuki reaction. *Chem. Methodol.* **6**, 629–638. https://doi.org/10.22034/chemm.2022.339192.1496 (2022).
5. Yu, Y., Ren, Y., Shen, W., Deng, H. & Gao, Z. Applications of metal organic frameworks as stationary phases in chromatography. *Trends Anal. Chem.* **50**, 33–41. https://doi.org/10.1016/j.trac.2013.04.014 (2013).
6. Pettinari, C., Marchetti, F., Mosca, N., Tosi, G. & Drozdov, A. Application of metal–organic frameworks. *Polym. Int.* **66**, 731–744. https://doi.org/10.1002/pi.5315 (2017).
7. Safaei, M. *et al.* A review on metal-organic frameworks: Synthesis and applications. *TrAC Trends Anal. Chem.* **118**, 401–425. https://doi.org/10.1016/j.trac.2019.06.007 (2019).
8. Petrov, V. V., Nazarova, T. N., Korolev, A. N. & Kopilova, N. F. Thin sol–gel SiO_2–SnO_x–AgO_y films for low temperature ammonia gas sensor. *Sens. Actuators B Chem.* **133**, 291–295. https://doi.org/10.1016/j.snb.2008.02.026 (2008).
9. Sanli, E., Uysal, B. Z. & Aksu, M. L. The oxidation of $NaBH_4$ on electrochemicaly treated silver electrodes. *Int. J. Hydrogen Energy.* **33**, 2097–2104. https://doi.org/10.1016/j.ijhydene.2008.01.049 (2008).
10. Ida, Y. *et al.* Direct electrodeposition of 1.46 eV bandgap silver (I) oxide semiconductor films by electrogenerated acid. *Chem. Mater.* **20**, 1254–1256. https://doi.org/10.1021/cm702865r (2008).
11. Li, W. X., Stampfl, C. & Scheffler, M. Insights into the function of silver as an oxidation catalyst by ab initio atomistic thermodynamics. *Phys. Rev. B* **68**, 165412. https://doi.org/10.1103/PhysRevB.68.165412 (2003).
12. Wang, Y. H. & Gu, H. Y. Hemoglobin co-immobilized with silver–silver oxide nanoparticles on a bare silver electrode for hydrogen peroxide electroanalysis. *Microchim. Acta* **164**, 41–47. https://doi.org/10.1007/s00604-008-0029-y (2009).
13. Sahoo, P. K. *et al.* Synthesis of silver nanoparticles using facile wet chemical route. *Def. Sci. J.* **59**, 447–455 (2009).
14. Popa, M., Pradell, T., Crespo, D. & Calderon-Moreno, J. M. Stable silver colloidal dispersions using short chain polyethylene glycol. *Colloids Surf. A.* **303**, 184–190. https://doi.org/10.1016/j.colsurfa.2007.03.050 (2007).
15. Neetha, M., Rohit, K. R., Saranya, S. & Anilkumar, G. Zinc-catalysed multi-component reactions: An overview. *ChemistrySelect* **5**, 1054–1070. https://doi.org/10.1002/slct.201904146 (2020).

16. Shilpa, T., Dhanya, R., Saranya, S. & Anilkumar, G. An overview of rhodium-catalysed multi-component reactions. *ChemistrySelect* **5**, 898–915. https://doi.org/10.1002/slct.201904441 (2020).
17. Bhaskaruni, S. V., Maddila, S., Gangu, K. K. & Jonnalagadda, S. B. A review on multi-component green synthesis of N-containing heterocycles using mixed oxides as heterogeneous catalysts. *Arab. J. Chem.* **13**, 1142–1178. https://doi.org/10.1016/j.arabjc.2017.09.016 (2020).
18. Maleki, B., Jamshidi, A., Peiman, S. & Housaindokht, M. R. Tri-vanadium substituted dawson-type heteropolytungstate nanocomposite (g-C_3N4/Fe_3O_4@ $P_2W_{15}V_3$) as a novel, green, and recyclable nanomagnetic catalyst in the synthesis of tetrahydrobenzo [b] pyrans. *Polycycl. Aromat. Compd.* **1**, 1–17. https://doi.org/10.1080/10406638.2023.2184398 (2023).
19. Alinezhad, H., Tajbakhsh, M., Maleki, B. & PourshabanOushibi, F. Acidic ionic liquid [H-NP] HSO_4 promoted one-pot synthesis of dihydro-1H-indeno [1, 2-b] pyridines and polysubstituted imidazoles. *Polycycl. Aromat. Compd.* **40**, 1485–1500. https://doi.org/10.1080/10406638.2018.1557707 (2020).
20. Udgire, S., Gaikwad, M. & Patil, P. Bi $(OTf)_3$ as a highly potent catalyst for the synthesis of Mannich bases under milder conditions. *Appl. Organomet. Chem.* **2**, 31–38 (2022).
21. Naderi, S., Sandaroos, R., Peiman, S. & Maleki, B. Novel crowned cobalt(II) complex containing an ionic liquid: A green and efficient catalyst for the one-pot synthesis of chromene and xanthene derivatives starting from benzylic alcohols. *J. Phys. Chem. Solids* **180**, 111459. https://doi.org/10.1016/j.jpcs.2023.111459 (2023).
22. Saadati-Moshtaghin, H. R., Maleki, B., Tayebee, R., Kahrobaei, S. & Abbasinohoji, F. 6-Methylguanamine-supported $CoFe_2O_4$: An efficient catalyst for one-pot three-component synthesis of isoxazol-5 (4 H)-one derivatives. *Polycycl. Aromat. Compd.* **42**, 885–896. https://doi.org/10.1080/10406638.2020.1754865 (2022).
23. Maleki, B., Kahoo, G. E. & Tayebee, R. One-pot synthesis of polysubstituted imidazoles catalyzed by an ionic liquid. *Org. Prep. Proced. Int.* **47**, 461–472. https://doi.org/10.1080/00304948.2015.1088757 (2015).
24. Esmaili, S., Moosavi-Zare, A. R., Khazaei, A. & Najafi, Z. Synthesis of novel pyrimido [4, 5-b] quinolines containing benzyloxy and 1, 2, 3-triazole moieties by DABCO as a basic catalyst. *ACS Omega* **7**, 45314–45324. https://doi.org/10.1021/acsomega.2c05896 (2020).
25. Petrova, K. V., Stec, D. F., Voehler, M. & Rizzo, C. J. Synthesis of the four stereoisomers of 2, 3-epoxy-4-hydroxynonanal and their reactivity with deoxyguanosine. *Org. Biomol. Chem.* **9**, 1960–1971. https://doi.org/10.1039/C0OB00546K (2011).
26. Saha, A., Payra, S. & Banerjee, S. One-pot multicomponent synthesis of highly functionalized bio-active pyrano [2, 3-c] pyrazole and benzylpyrazolyl coumarin derivatives using ZrO_2 nanoparticles as a reusable catalyst. *Green Chem.* **17**, 2859–2866. https://doi.org/10.1039/C4GC02420F (2015).
27. Luo, Y. *et al.* Design, synthesis and bioevaluation of N-trisubstituted pyrimidine derivatives as potent aurora A kinase inhibitors. *Eur. J. Med. Chem.* **78**, 65–71. https://doi.org/10.1016/j.ejmech.2014.03.027 (2014).
28. Toledo, M. A. *et al.* Discovery of a novel series of orally active nociceptin/orphanin FQ (NOP) receptor antagonists based on a dihydrospiro (piperidine-4, 7′-thieno [2, 3-c] pyran) scaffold. *J. Med. Chem.* **57**, 3418–3429. https://doi.org/10.1021/jm500117r (2014).
29. Sangani, C. B. *et al.* Design, synthesis and molecular modeling of pyrazole–quinoline–pyridine hybrids as a new class of antimicrobial and anticancer agents. *Eur. J. Med. Chem.* **76**, 549–557. https://doi.org/10.1016/j.ejmech.2014.01.018 (2014).
30. Abdelrazek, F. M., Metz, P., Metwally, N. H. & El-Mahrouky, S. F. Synthesis and molluscicidal activity of new cinnoline and pyrano [2, 3-c] pyrazole derivatives. *Arch. Pharm.* **339**, 456–460. https://doi.org/10.1002/ardp.200600057 (2006).
31. Foloppe, N. *et al.* Identification of chemically diverse Chk1 inhibitors by receptor-based virtual screening. *Bioorg. Med. Chem.* **14**, 4792–4802. https://doi.org/10.1016/j.bmc.2006.03.021 (2006).
32. Thumar, N. J. & Patel, M. P. Synthesis and in vitro antimicrobial evaluation of 4H-pyrazolopyran-benzopyran and naphthopyran derivatives of 1H-pyrazole. *Arkivoc* **13**, 363–380 (2009).
33. Yousefi, A. *et al.* Novel curcumin-based pyrano [2, 3-d] pyrimidine anti-oxidant inhibitors for α-amylase and α-glucosidase: Implications for their pleiotropic effects against diabetes complications. *Int. J. Biol. Macromol.* **78**, 46–55. https://doi.org/10.1016/j.ijbiomac.2015.03.060 (2015).
34. Esmaeili, A. A., Salehan, F., Habibi, A. & Fakhari, A. R. Efficient synthesis of novel pyrano [2, 3-d] pyrido [1, 2-a] pyrimidine derivatives via isocyanide-based three-component reactions. *Tetrahedron Lett.* **57**, 100–102. https://doi.org/10.1016/j.tetlet.2015.11.073 (2016).
35. Mohamed, N. R., Khaireldin, N. Y., Fahmyb, A. F. & El-Sayeda, A. A. F. Facile synthesis of fused nitrogen containing heterocycles as anticancer agents. *Der Pharm. Chem.* **2**, 400–417 (2010).
36. Wang, J. L. *et al.* Structure-based discovery of an organic compound that binds Bcl-2 protein and induces apoptosis of tumor cells. *Proc. Natl. Acad. Sci. USA* **97**, 7124–7129. https://doi.org/10.1073/pnas.97.13.7124 (2000).
37. Prasad, Y. R., Rao, A. L., Prasoona, L., Murali, K. & Kumar, P. R. Synthesis and antidepressant activity of some 1, 3, 5-tripheny-2-pyrazolines and 3-(2\\-hydrox; ynaphthalen-1\\-yl)-1, 5-diphenyl-2-pyrazolines. *Bioorg. Med. Chem. Lett.* **15**, 5030–3034 (2005).
38. Ellingboe, J. W. & Princeton, N. *J. Chem. Abs.* **124** (1996).
39. Ahluwalia, V. K., Dahiya, A. & Garg, V. Reaction of 5-amino -4- formyl-3-methyl (or phenyl)-l- phenyl-lH- pyrazoles with active methylene compounds: Synthesis of fused heterocyclic rings. *Indian J. Chem.* **36**, 88–90 (1997).
40. Agarwal, A., Goyal, N., Chauhan, P. M. & Gupta, S. Dihydropyrido [2, 3-d] pyrimidines as a new class of antileishmanial agents. *Bioorg. Med. Chem.* **13**, 6678–6684. https://doi.org/10.1016/j.bmc.2005.07.043 (2005).
41. Kolla, V. E., Deyanov, A. B., Nazmetdinov, F. Y., Kashina, Z. N. & Drovosekova, L. P. Investigation of the anti-inflammatory and analgesic activity of 2-substituted 1-aryl-6-carboxy (carbethoxy)-7-methyl-4-oxo-1, 4-dihydropyrido [2, 3-d] pyrimidines. *Pharm. Chem. J.* **27**, 635–636. https://doi.org/10.1007/BF00780584 (1993).
42. Bagley, M. C. *et al.* Microwave-assisted synthesis of pyrimidine libraries. *QSAR Comb. Sci.* **23**, 859–867. https://doi.org/10.1002/qsar.200420044 (2004).
43. Deyanov, A. B. *et al.* Synthesis and biological activity of amides and nitriles of 2-arylamino-5-carboxy (carbethoxy)-6-methylnicotinic acids and 1-aryl-6-carbethoxy-7-methyl-4-oxo-1, 4-dihydropyrido [2, 3-d] pyrimidines. *Pharm. Chem. J.* **25**, 248–250. https://doi.org/10.1007/BF00772106 (1991).
44. Bystryakova, I. D. *et al.* Synthesis and biological activity of pyridol [2, 3-d] pyrimidines. *Pharm. Chem. J.* **25**, 874–876. https://doi.org/10.1007/BF00778976 (1991).
45. Furuya, S. & Ohtaki, T. Inventors; Eur. Pat. Appl. EP. 608565. *Chem. Abstr.* **121**, 205395 (1994).
46. Rosowsky, A., Mota, C. E. & Queener, S. F. Synthesis and antifolate activity of 2, 4-diamino-5, 6, 7, 8-tetrahydropyrido [4, 3-d] pyrimidine analogues of trimetrexate and piritrexim. *J. Heterocycl. Chem.* **32**, 335–340. https://doi.org/10.1002/jhet.5570320155 (1995).
47. Ahanthem, D., Singh, S. M. & Laitonjam, W. S. Synthesis, Antimicrobial and Antioxidant Activities of Novel 7-thioxo-4, 6, 7, 8-tetrahydro-pyrazolo [4′, 3′: 5, 6] pyrano [2, 3-d] pyrimidin-5 (1H)-ones derived by SDS catalyzed multicomponent reactions in aqueous micellar media. *J. Nat. Prod.* **8**, 228–238. https://doi.org/10.2174/2210315508666180327143107 (2018).
48. Heravi, M. M., Mousavizadeh, F., Ghobadi, N. & Tajbakhsh, M. A green and convenient protocol for the synthesis of novel pyrazolopyranopyrimidines via a one-pot, four-component reaction in water. *Tetrahedron Lett.* **55**, 1226–1228. https://doi.org/10.1016/j.tetlet.2014.01.004 (2014).

49. Tipale, M. R., Khillare, L. D., Deshmukh, A. R. & Bhosle, M. R. An efficient four component domino synthesis of pyrazolopyranopyrimidines using recyclable choline chloride: Urea deep eutectic solvent. *J. Heterocycl. Chem.* **55**, 716–728. https://doi.org/10.1016/j.tetlet.2014.01.004 (2018).
50. Sadjadi, S., Heravi, M. M. & Daraie, M. Heteropolyacid supported on amine-functionalized halloysite nano clay as an efficient catalyst for the synthesis of pyrazolopyranopyrimidines via four-component domino reaction. *Res. Chem. Intermed.* **43**, 2201–2214. https://doi.org/10.1007/s11164-016-2756-8 (2017).
51. Bakherad, M., Doosti, R., Keivanloo, A., Gholizadeh, M. & Amin, A. A new, simple, catalyst-free method for the synthesis of pyrazolopyranopyrimidines in magnetized water. *Lett. Org. Chem.* **14**, 510–516. https://doi.org/10.2174/1570178614666170511170329 (2017).
52. Heravi, M. M. & Daraie, M. A novel and efficient five-component synthesis of pyrazole based pyrido [2, 3-d] pyrimidine-diones in water: A triply green synthesis. *Molecules* **21**, 441–453. https://doi.org/10.3390/molecules21040441 (2016).
53. Dastkhoon, S., Tavakoli, Z., Khodabakhshi, S., Baghernejad, M. & Abbasabadi, M. K. Nanocatalytic one-pot, four-component synthesis of some new triheterocyclic compounds consisting of pyrazole, pyran, and pyrimidinone rings. *New J. Chem.* **39**, 7268–7271. https://doi.org/10.1039/C5NJ01046B (2015).
54. Li, X. T., Zhao, A. D., Mo, L. P. & Zhang, Z. H. Meglumine catalyzed expeditious four-component domino protocol for synthesis of pyrazolopyranopyrimidines in aqueous medium. *RSC Adv.* **4**, 51580–51588. https://doi.org/10.1039/C4RA08689A (2014).
55. Maleki, A., Jafari, A. A. & Yousefi, S. Green cellulose-based nanocomposite catalyst: Design and facile performance in aqueous synthesis of pyranopyrimidines and pyrazolopyranopyrimidines. *Carbohydr. Polym.* **175**, 409–416. https://doi.org/10.1016/j.carbpol.2017.08.019 (2017).
56. Rigi, F. & Shaterian, H. R. Silica-supported ionic liquids prompted one-pot four-component synthesis of pyrazolopyranopyrimidines, 3-methyl-4-aryl-4, 5-dihydro-1 H-pyrano [2, 3-c] pyrazol-6-ones, and 1, 6-diamino-2-oxo-1, 2, 3, 4-tetrahydropyridine-3, 5-dicarbonitriles. *Polycycl. Aromat. Compd.* **37**, 314–326. https://doi.org/10.1080/10406638.2015.1112821 (2017).
57. Rigi, F. & Shaterian, H. R. Magnetic nanoparticle supported ionic liquid assisted green synthesis of pyrazolopyranopyrimidines and 1, 6-diamino-2-oxo-1, 2, 3, 4-tetrahydropyridine-3, 5-dicarbonitriles. *J. Chin. Chem. Soc.* **63**, 557–561. https://doi.org/10.1002/jccs.201500407 (2016).
58. Khodabakhshi, S., Rashidi, A., Tavakoli, Z., Baghernejad, M. & Yadegari, A. The first catalytic application of oxidized carbon nanotubes in a four-component synthesis of fused heterocycles. *Monatsh. Chem.* **147**, 791–795. https://doi.org/10.1007/s00706-015-1532-6 (2016).
59. Ziarani, G. M., Aleali, F., Lashgari, N., Badiei, A. & Soorki, A. A. Efficient synthesis and antimicrobial evaluation of pyrazolopyranopyrimidines in the presence of SBA-Pr-SO_3H as a nanoporous acid catalyst. *Iran. J. Pharm. Res.* **17**, 525 (2018).
60. Ganesan, A., Kothandapani, J. & Subramaniapillai, S. G. Extending the scope of oleic acid catalysis in diversity-oriented synthesis of chromene and pyrimidine-based scaffolds. *RSC Adv.* **6**, 20582–20587. https://doi.org/10.1039/C6RA02507B (2016).
61. Nasresfahani, Z. & Kassaee, M. Z. Cu–immobilized mesoporous silica nanoparticles [Cu^{2+}@ MSNs-$(CO_2^-)_2$] as an efficient nanocatalyst for one-pot synthesis of pyrazolopyranopyrimidines in water. *ChemistrySelect* **2**, 9642–9646. https://doi.org/10.1002/slct.201701452 (2017).
62. Zhou, W. *et al.* Ag_2O/TiO_2 nanobelts heterostructure with enhanced ultraviolet and visible photocatalytic activity. *ACS Appl. Mater. Interfaces* **2**, 2385–2392. https://doi.org/10.1021/am100394x (2010).
63. Shahryari, T. *et al.* A controllable procedure for removing Navicula algae from drinking water using an ultrasonic-assisted electrospun method for highly efficient synthesis of Co-MOF/PVA polymeric network. *J. Appl. Phys.* **128**, 396. https://doi.org/10.1007/s00339-022-05524-x (2022).
64. Sargazi, G., Afzali, D., Ghafainazari, A. & Saravani, H. Rapid synthesis of cobalt metal organic framework. *J. Inorg. Organomet. Polym. Mater.* **24**, 786–790. https://doi.org/10.1007/s10904-014-0042-z (2014).
65. Aziz, A. *et al.* Structural, morphological and optical investigations of silver nanoparticles synthesized by sol-gel auto-combustion method. *Dig. J. Nanomater. Biostruct.* **13**, 679–683 (2018).
66. Murinzi, T. W., Hosten, E. & Watkins, G. M. Synthesis and characterization of a cobalt-2, 6-pyridinedicarboxylate MOF with potential application in electrochemical sensing. *Polyhedron* **137**, 188–196. https://doi.org/10.1016/j.poly.2017.08.030 (2017).
67. Keshavarz, M., Mamaghani, M., Dekamin, M. G. & Nikpassand, M. Tetramethylguanidine-functionalized nanosize γ-Al_2O_3 as a novel and efficient catalyst for the four-component synthesis of pyrazolopyranopyrimidine derivatives. *J. Iran. Chem. Soc.* **18**, 1419–1431. https://doi.org/10.1007/s13738-020-02123-6 (2021).
68. Akolkar, S. V., Kharat, N. D., Nagargoje, A. A., Subhedar, D. D. & Shingate, B. B. Ultrasound-assisted β-cyclodextrin catalyzed one-pot cascade synthesis of pyrazolopyranopyrimidines in water. *Catal. Lett.* **150**, 450–460. https://doi.org/10.1007/s10562-019-02968-4 (2020).
69. Rostami, H. & Shiri, L. $CoFe_2O_4$@ SiO_2-PA-CC-guanidine MNPs as an efficient catalyst for the one-pot four-component synthesis of pyrazolopyranopyrimidines. *ChemistrySelect* **4**, 8410–8415. https://doi.org/10.1002/slct.201901925 (2019).
70. Kardooni, R. & Kiasat, A. R. A green, catalyst-free synthesis of pyrazolopyranopyrimidines in polyethylene glycol as a biodegradable medium at ambient temperature. *Mol. Divers.* **23**, 639–649. https://doi.org/10.1007/s11030-018-9898-0 (2019).
71. Bakherad, M., Doosti, R., Mirzaee, M. & Jadidi, K. Synthesis of pyrazolopyranopyrimidines catalyzed by caffeine supported on boehmite nanoparticles and their evaluation for anti-bacterial activities. *Iran. J. Catal.* **7**, 27–35 (2017).
72. Rostami, A., Pourshiani, O., Navasi, Y., Darvishi, N. & Saadati, S. Magnetic nanoparticle-supported DABCO tribromide: A versatile nanocatalyst for the synthesis of quinazolinones and benzimidazoles and protection/deprotection of hydroxyl groups. *New J. Chem.* **41**, 9033–9040. https://doi.org/10.1039/C7NJ00479F (2017).
73. Patil, P. *et al.* [MerDABCO-SO_3H] Cl catalyzed synthesis, antimicrobial and antioxidant evaluation and molecular docking study of pyrazolopyranopyrimidines. *J. Mol. Struct.* **1242**, 130672. https://doi.org/10.1016/j.molstruc.2021.130672 (2021).
74. Mahmoudi, Z., Ghasemzadeh, M. A. & Kabiri-Fard, H. Fabrication of UiO-66 nanocages confined bronsted ionic liquids as an efficient catalyst for the synthesis of dihydropyrazolo [4′, 3′: 5, 6] pyrano [2, 3-d] pyrimidines. *J. Mol. Struct.* **1194**, 1–10. https://doi.org/10.1016/j.molstruc.2019.05.079 (2019).

Acknowledgements

The authors appreciate the Islamic Azad University (Kerman Branch), for supporting this research.

Author contributions

G.H.: Investigation Roles/Writing—original draft. E.S.: conceptualization, data curation, formal analysis, investigation, methodology, project administration, Resources, Supervision, Validation, Visualization, Writing—review & editing. S.A.A. and M.Y.: formal analysis, methodology, supervision, validation, visualization, Writing—review & editing. This article has been read by all authors and agreed to be published.

Funding

The authors received no specific funding for this work.

Competing interests
The authors declare no competing interests.

Additional information
Supplementary Information The online version contains supplementary material available at https://doi.org/10.1038/s41598-023-44667-6.

Correspondence and requests for materials should be addressed to E.S.

Reprints and permissions information is available at www.nature.com/reprints.

Publisher's note Springer Nature remains neutral with regard to jurisdictional claims in published maps and institutional affiliations.